Author Manuscript

Author Manuscript

Author Manuscript

Author Manuscript

HHS Public Access

Author manuscript

Oral Oncol. Author manuscript; available in PMC 2016 May 01.

Published in final edited form as:

Oral Oncol. 2015 May ; 51(5): 476–482. doi:10.1016/j.oraloncology.2015.01.012.

Orthotopic non-metastatic and metastatic oral cancer mouse models ⋆

Manish V. Bais*, **Maria Kukuruzinska**, and **Philip C. Trackman**

Boston University Henry M. Goldman School of Dental Medicine, Department of Molecular and Cell Biology, Boston, MA 02118, United States

SUMMARY

Oral cancer is characterized by high morbidity and mortality with a predisposition to metastasize to different tissues, including lung, liver, and bone. Despite progress in the understanding of mutational profiles and deregulated pathways in oral cancer, patient survival has not significantly improved over the past decades. Therefore, there is a need to establish *in vivo* models that recapitulate human oral cancer metastasis to evaluate therapeutic potential of novel drugs. Here we report orthotopic tongue cancer nude mouse models to study oral cancer growth and metastasis using human metastatic (UMSCC2) and non-metastatic (CAL27) cell lines, respectively. Transduction of these cell lines with lentivirus expressing red fluorescent protein (DsRed) followed by injection into tongues of immunodeficient mice generated orthotopic tongue tumors that could be monitored for growth and metastasis by fluorescence measurement with an *in vivo* Imaging System (IVIS 200). The growth rates of CAL27-DsRed induced tumors were higher than UMSCC2-DsRed tumors after day 15, while UMSCC2-DsRed tumors revealed metastasis beginning on day 21. Importantly, UMSCC2 tumors metastasized to a number of tissues including the submandibular gland, lung, kidney, liver, and bone. Further, immunohistochemical analyses of tongue tumors induced by CAL27 and UMSCC2 cells revealed elevated expression of components of protumorigenic pathways deregulated in human cancers, including Cyclin D1, PCNA, Ki-67, LSD1, LOXL2, MT-MMP1, DPAGT1, E-cadherin, OCT4A, and H3K4me1/2. These orthotopic mouse models are likely to be useful tools for gaining insights into the activity and mechanisms of novel oral cancer drug candidates.

Keywords

Oral cancer; Orthotopic tumors metastasis; Mouse models

⋆Supported by Boston University Henry M. Goldman School of Dental Medicine seed funding to Manish Bais; and the Oral Cancer Research Initiative seed funding to Manish Bais and Philip Trackman.

© 2015 Elsevier Ltd. All rights reserved

* Corresponding author at: Boston University, Henry M. Goldman School of Dental Medicine, 700 Albany Street, W-201, Boston, MA 02118, United States. Tel.: +1 617 638 4004. bmanish@bu.edu (M.V. Bais)..

Conflict of interest statement

The authors declare that they have no conflicts of interest.

Author Manuscript Author Manuscript Author Manuscript Author Manuscript

Introduction

Oral squamous cell carcinoma (OSCC), accounts for the majority of head and neck cancers and ranks as one of the most common cancers in the world [1,2]. In contrast to other cancers, oral cancer statistics are dismal: half of oral cancers are not diagnosed until the cancer has spread to nearby tissues, at which stage the 5-year survival rate is approximately 50% [3,4]. Oral cancer arises from the neoplasms of the oral cavity with more than 90% of cases classified as squamous cell carcinomas (SCC). Treatment for OSCC frequently involves a combination of surgery, radiotherapy, and chemotherapy [5]. Despite these dire statistics and disease morbidity, OSCC is one of the most understudied cancers with little information known about the molecular mechanisms underlying its etiology and progression. Likewise, no molecular biomarkers have been identified to inform decisions about either timely diagnosis or treatment. Studies to date have shown that OSCC's primary tumor growth and metastasis are controlled by numerous factors, including the microenvironment, and different biologics have been under development for treating OSCC. A reliable model to evaluate the effects of these candidate new therapeutics is needed to gain insights into their preclinical effectiveness.

Current OSCC mouse models include subcutaneous xenografts, orthotopic injections and genetically engineered models [6–9]. Subcutaneous mouse xenografts generally do not recapitulate advanced local–regional or distant metastatic disease. Orthotopic transplantation of tumor cells remains a reproducible and reliable methodology for studying mechanisms and potential therapeutic applications, since phenotypic properties of metastatic cells are governed by the expression of genes that are regulated by interactions with the relevant organ-specific microenvironment [10]. However, these orthotopic OSCC mouse models rely on the use of bioluminescence, which is fraught with transient and variable signals, and they exhibit limited metastasis [11,12] that do not reflect many sites observed in human OSCC [13–17].

The goal of the present study is to establish mouse models that primarily reflect tumor growth and metastasis for mechanistic and therapeutic studies. We have generated an orthotopic oral cancer nude mouse model using either non-metastatic CAL27 cells or metastatic UMSCC2 cell lines expressing red fluorescent protein (DsRed) that can be imaged *in vivo*. Injection of CAL27 cells into the tongues of nude mice induced local tumor growth with no evidence of spread to internal organs, whereas UMSCC2 cells induced both a primary tumor and extensive metastasis. We present evidence that these animal models provide important insights into the mechanism OSCC growth and metastasis, and will permit relatively rapid screening for the therapeutic potential of small molecules or more complex biologics in preclinical studies.

Materials and methods

Stable cell line generation

Non-metastatic CAL27 cells were obtained from ATCC and Dr. Maria Kukuruzinska's laboratory at the Boston University Henry M. Goldman School of Dental Medicine. The metastatic cell line (UMSCC2) cells were generously provided by Dr. Roberto Weigert's

Author Manuscript Author Manuscript Author Manuscript Author Manuscript

laboratory at NIDCR, Bethesda, MD. These cells were grown under standard conditions (DMEM, 10% FBS, 1% penicillin-–streptomycin). The plasmid for DsRed protein expression (pHAGE-EF1a-DsRed-UBC-GFP) was provided by Dr. Darrell Kotton's laboratory at the Boston University School of Medicine. In order to visualize these cells *in vivo*, cells were infected with lentivirus particles expressing DsRed protein at a multiplicity of infection of 25 according to a standard protocol [18] to generate CAL27-DsRed and UMSCC2-DsRed cells. The expression of DsRed protein in these cells was confirmed by fluorescence microscopy.

Orthotopic injection of OSCC cells into nude mice

All experiments were performed as approved by Boston University Medical Center IACUC. CAL27-DsRed and UMSCC2-DsRed cells were trypsinized and suspended in serum-free DMEM media. These cells (0.5×10^6 cells in 40 μl per tongue) were injected into two month old nude mice (NCr nu/nu, n = 5/group; Taconic Farms, Hudson, NY), in respective groups after anesthetizing with 4% isoflurane. Mice in the control group were injected with vehicle only. Caliper measurements were performed at regular intervals to monitor the volumes of all tumors. Tumors were harvested at sacrifice, weighed and either snap frozen, ground to a fine powder in liquid nitrogen and then extracted for Western blotting or processed for histology and immunohistochemistry.

IVIS imaging

Mice were imaged for DsRed protein expression using an IVIS 200 system (Xenogen, Alameda, CA, USA) [19]. Anesthesia was administered in an induction chamber with 2.5% isoflurane in 100% oxygen at a flow rate of 1 L/min and then maintained with a 1.5% mixture at 0.5 L/min. The fluorescence signals were optimized for DsRed protein at excitation 570 and emission 620. Fluorescence region of interest (ROI) data are the calibrated, normalized fluorescence efficiency $(p/s/cm^2/sr)/(\mu W/cm^2)$ as per the instructions (Perkin Elmer, USA). The data are reported as normalized fluorescence intensity (FU) from a defined region of interest for oral tongue tumors or systemic metastases compared to control vehicle-injected mice.

Western blots

Tumor samples were extracted into SDS PAGE sample buffer (0.1 mM Tris–HCl, 4% SDS, 10% glycerol, 5% β-mercaptoethanol) and boiled for three to five minutes. Protein concentrations were determined using Nano Orange assay kits (Molecular Probes, Eugene, OR, USA). Samples of approximately 20 μg of protein were obtained from extracts of 3 pooled tumors per experimental group and were subjected to 10% SDS PAGE and Western blotting with primary antibodies from Cell Signaling Technology (Danvers, MA, USA). The antibodies used were Cyclin D1 (#2926), PCNA (#2586), LSD1 (#2139), Mono-Methyl-Histone H3 Lysine 4 (H3K4me1) (#9723) and the normalization control β-actin (#4970). Horse radish peroxidase-coupled anti-rabbit and antimouse secondary antibodies were purchased from Cell Signaling Technology (Danvers, MA, USA; 7074 and 7076, respectively).

Author Manuscript Author Manuscript Author Manuscript Author Manuscript

Immunostaining

All tumors were harvested at sacrifice and then fixed in 4% paraformaldehyde overnight, and placed in phosphate buffered saline overnight at 4°°C. Tongue tumor tissue sections were made and subjected to immunohistochemistry. Three tumors, 3 to 4 sections per tumor, were used for immunohistochemistry staining analysis using rabbit antibodies for Ki-67 (Abcam Inc.; ab15580), LSD1 (Cell Signaling Technology #2139) OCT4A (Cell Signaling Technology #2840) E-cadherin (BD Transduction laboratories, #610181), MT-MMP1 (Abcam Inc;ab51074) DPAGT1 (Covance Research Products, Inc [20]) and LOXL2 (GeneTex #GTX105085).

Statistical analysis

All experiments were analyzed using two way ANOVA with Bonferroni post hoc analysis or Student's *t*-test (Graph Pad Prism 5 software, La Jolla, CA) as indicated in the figure legends.

Results

Orthotopic implantation of CAL27 cells into tongues induces tumor growth

In order to study the growth of orthotopic tumors, we injected CAL27-DsRed cells into the mouse tongue. Caliper measurements at regular intervals showed that CAL27 tumors exponentially grew for first 18 days and then at a slightly slower rate up to 25 ± 6 mm^3 by day 31. IVIS imaging of these mice shows that on day 24, the tumors are localized to the anterior part of the tongue, and tumors continued to grow until day 31 (Fig. 1). The data also show that the average fluorescence intensity on day 24 was 2.3×10^8 units which more than doubled to 7.1×10^8 units by day 31. No evidence for metastasis to distant tissues was observed.

Orthotopic implantation of UMSCC2 cells into tongues induces tumor growth and metastasis

Human OSCC metastasizes to a number of organs including lung, liver, bone, intestine and other tissues [13–17]. To determine if UMSCC2-induced mouse tumors metastasize to organs similar to the sites in human OSCC, we followed their growth and metastasis *in vivo* for 31 days. Interestingly, caliper measurements showed that CAL27-derived tumors grew larger (25 ± 6 mm^3) compared to UMSCC2 tumors (20 ± 5 mm^3), and they displayed higher fluorescence intensity (Figs. 1 and 2). This finding may be related to the metastatic character of UMSCC2 cells.

As shown in Fig. 2, UMSCC2 cell injection induces tongue tumors by day 24 with some evidence of metastasis. Further metastases were detected by day 31. Fluorescence intensity on day 24 was 6.3×10^7 units, and it increased to 11×10^7 units on day 31 in the orofacial region. A comparative analysis of systemic fluorescence showed that fluorescence intensity increased more than 4-fold from 4.7×10^7 on day 24 to 19×10^7 on day 31. To further confirm these results, we dissected internal organs and imaged with IVIS to find fluorescence in the tongue, sublingual tissues, lung, kidneys, liver, intestine and bone, but

Author Manuscript Author Manuscript Author Manuscript Author Manuscript

not in the heart. Thus, UMSCC2 metastasizes by 24 days post-injection which ultimately spreads to a variety of internal organs.

Characterization of CAL27- and UMSCC2-induced tumors

To evaluate changes in the expression and localization of selected components of oncogenic pathways in primary tumors from CAL27 and UMSCC2 cells, we carried out Western blot analyses on tongue tumor tissue extracts. Results showed that while both CAL27- and UMSCC2-derived tumors expressed Cyclin D1 and proliferating cell nuclear antigen (PCNA), the UMSCC2-induced tumors displayed higher expression of these proliferation markers compared to CAL27 cell-derived tumor tissues. This was supported by immunostaining of Ki-67, which also showed increased expression in CAL27- and UMSCC2-derived tongue tumors compared to vehicle injection (Fig. 3). Further, aberrant up-regulation of epigenetic regulators, such as lysine specific demethylase (LSD1) and methylated histone H3K4, occurs in most human carcinomas [21–25]. Accordingly, Western blot analyses of CAL27 and UMSCC2 tumors revealed increased expression of LSD1 and H3K4me1 in UMSCC2-induced tumors (Fig. 3). Similarly, immunostaining analyses showed higher expression of LSD1 in UMSCC2 tumors (Fig. 3).

As expected for epithelial tumors, immunostaining analyses of CAL27 and UMSCC2 tumors showed that both tissues expressed E-cadherin. We have shown previously that human OSCC is characterized by deregulated E-cadherin adhesion and increased expression of the N-glycosylation regulating gene, DPAGT1 [20,26,27]. Compared to CAL27-induced tumors, the UMSCC2 tumors exhibited more prominent staining intensity for the DPAGT1 protein, GPT, in subsets of tumor cells. Since increased N-glycosylation is associated with primitive cell surface markers and cell “stemness”, we also examined these tumors for OCT4, a stem cell marker, whose expression is a feature of various cancers and has been implicated to be a first step in tumor initiation [24,25]. Data in Fig. 4 show clusters of OCT4A positive cells in CAL27-induced tumors. In contrast, in UMSCC2-derived tumors, expression of OCT4A was found in more dispersed cells.

Importantly, the UMSCC2 tumors were characterized by dramatic changes in the adjacent tumor stroma. UMSCC2-induced tumors displayed much higher expression of the extracellular matrix (ECM) enzymes, lysyl oxidase like-2 (LOXL2) and MT-MMP1, compared to CAL27 cells (Fig. 4). Both enzymes are critical drivers of the ECM remodeling, with LOXL2 being aligned with cancer associated fibroblasts and an indicator of poor prognosis in human oral cancer [28–30] and MT-MMP1 a metalloproteinase with a role in proliferation, migration and invasion [31–33]. Thus, up-regulation of LOXL2 and MT-MMP1 observed in Fig. 4 is consistent with characteristics of human oral cancer and tumorigenesis in general.

Discussion

OSCC frequently metastasizes to the lymph nodes and distant organs, such as lung, bone, and liver [13–17]. Clinically, distant metastasis ranges from 20% to 40% leading to poor survival and failure of surgical, chemotherapeutic and radiation therapy interventions. Organ-specific microenvironments are important contributors to metastasis, and reliable

Author Manuscript Author Manuscript Author Manuscript Author Manuscript

orthotopic oral cancer models are required to study mechanisms of cancer initiation, progression, and metastasis. In addition, these models play a critical role in the initial evaluation of novel therapeutics [10]. Implantation of human oral cancer cell lines into oral tissues has been shown to provide a superior model for the study of metastasis compared to xenografts. Orthotopic implantation of OSCC cells has advantages in that it mimics the processes involved in local invasion and displays high rates of spontaneous tumor metastasis [9,34]. Although there are several models of tongue tumors, they have been reported to metastasize only to lymph nodes and lung [13–17]. While the carcinogenic 4-nitroquinoline-1-oxide (4NQO) model has been reported to recapitulate premalignant and malignant stages of OSCC, the 4NQO model requires more than 2 to 4 months to develop primary tumors [35,36] and detection of premalignant lesions or early SCC within the oral cavity of the test animals can be difficult with limited metastasis to lymph nodes and lung [37]. Here, we report two oral tongue cancer models for studies of tumor growth and metastasis, where the metastatic tumor spreads to several internal organs, and can be followed by noninvasive *in vivo* imaging using DsRed protein expression. These models represent useful tools for studies of mechanisms of metastasis and for initial evaluation of novel therapeutics in preclinical studies.

Our tongue cancer CAL27 and UMSCC2 mouse models offer several advantages over the previously described models. First, they are based on the DsRed protein *in vivo* imaging rather than bioluminescence imaging. The latter signals require injection of D-luciferin for transient visualization, which is metabolized and may be degraded differently in each mouse. For example, luciferase enzyme activity requires ATP whose concentrations are highest in metabolically active cells. Under optimal conditions, bioluminescence provides sensitive detection with high signal-to-noise ratios and low auto-bioluminescence, but signals are transient and variable [33]. By contrast, DsRed protein expression is constitutive, stable, and does not require the injection of labile enzyme substrates for imaging. Second, our data show that although the volume and fluorescence intensity of CAL27-induced tongue tumors were higher than UMSCC2, the latter tumors metastasized readily to different internal organs, resembling the sites of metastases of OSCC in humans. This suggests that UMSCC2 cells migrate more readily out of the tongue tumor, thereby reducing the number of DsRed cells in the tongue. These results also support the notion observed in human OSCC that tumor size is not a reliable predictor of aggressive disease. The migrating UMSCC2 cells are likely to contain a proportion of cells with colonization potential that may be lacking in CAL27 cells. These features render the CAL27 and UMSCC2 tumor models applicable to studies of tumor initiation, expansion and metastasis.

Despite much progress in the understanding of the mutational landscape and deregulated cellular pathways in oral cancer, there is limited understanding of the regional and distant spread of OSCC. Our models are likely to offer additional tools for decoding molecular and cellular details driving this disease.

Initial analyses show that the expression of genes that function in cancer progression and metastasis is upregulated in metastatic UMSCC2-compared to CAL27-derived tumors. In particular, we found increased expression of proteins known to function as mediators of tumor initiation, development and progression including regulators of cell stemness,

Author Manuscript Author Manuscript Author Manuscript Author Manuscript

components of the cell cycle, the homeostatic N-glycosylation-intercellular adhesion network, epigenetic regulation, and of enzymes involved in the remodeling of the tumor stroma. While more studies focused on the mapping of pathway circuitries are required, these data suggest that at least some of these components may serve as therapeutic targets for the treatment of OSCC. Typically, the sensitivities of primary tumors and distant metastases to therapeutics are different, as microenvironments at metastatic sites in soft and hard tissues contribute to the efficacy of drugs. Therefore, while the drugs that are effective against primary oral cancer growth can also be used to inhibit metastasis, a successful outcome is often not accomplished. Here, our DsRed-labeled UMSCC2 model is likely to provide a valuable tool to evaluate efficacy of novel therapeutics in inhibiting both OSCC growth and metastasis.

We note that the interpretation of our findings with regard to tumor growth and metastasis is limited by the use of only two OSCC cell lines. Nonetheless, the molecular differences between these cell lines are consistent with observed phenotypes of tumor growth and metastasis. Further studies with a broader panel of cell lines accompanied by their molecular characterization will be needed to define molecular signatures of metastasis in these orthotopic tongue cancer mouse models.

Due to the paucity of effective treatments for OSCC, there is an urgent need for reproducible anti-oral cancer drug screening tools *in vivo*. Since our CAL27 and UMSCC2 models show altered expression of genes related to cell stemness, proliferation, N-glycosylation, adhesion, epigenetic regulation, and tumor stromal microenvironment, they can be used to test a range of drugs prior to evaluation in patient-derived primary tumors xenografts (PDX). PDX models have limitations such as lower engraftment rate and slow tumor growth, requiring at times multiple passages in mice to enrich for tumor cells. Further, PDX models are expensive and less reproducible [38], and orthotopic implantation of primary tumors tissue into the tongue and other sites in the oral cavity remains technically challenging. In this context, orthotopic DsRed-labeled UMSCC2- and CAL27-induced tumor models can be used as a tool to evaluate *in vivo* efficacy of various biologics or small molecule modulators as a first stage before evaluating in PDX models. In the future, molecular and phenotypic comparison of orthotopic UMSCC2 and CAL27 tumors with orthotopic PDX tumors could provide new insights into mechanisms of OSCC and candidate drugs.

Although various metastatic mouse models are available for OSCC, their relevance is diminished by limited metastasis beyond adjoining lymph nodes and submandibular tissues. We have successfully developed and characterized mouse models to study initiation, growth, progression and distant metastases of OSCC. These mouse models are also likely to be useful for an initial evaluation of biologics and small molecule inhibitors, and for the potential therapeutic application of a variety of candidate drugs in preclinical studies.

Acknowledgements

We are thankful to Dr. Roberto Weigert and Dr. Panomwat Amornphimoltham at NIDCR for providing their expertise and training regarding orthotopic tongue injections, and for providing us with the UMSCC2 cell line. We are grateful to Dr. Darrell Kotton for making the pHAGE-EF1a-DsRed-UBC-GFP construct available to us. The authors thank Michael Faibish for technical assistance with tissue sectioning. These studies were supported in part

Author Manuscript Author Manuscript Author Manuscript Author Manuscript

by Boston University Henry M. Goldman School of Dental Medicine seed funding to Manish Bais, and from the Oral Cancer Research Initiative at Boston University to Manish Bais and Philip Trackman.

References

[1]. Choi S, Myers JN. Molecular pathogenesis of oral squamous cell carcinoma: implications for therapy. J Dent Res. 2008; 87:14–32. [PubMed: 18096889]

[2]. Jemal A, Bray F, Center MM, Ferlay J, Ward E, Forman D. Global cancer statistics. CA Cancer J Clin. 2011; 61:69–90. [PubMed: 21296855]

[3]. Rothenberg SM, Ellisen LW. The molecular pathogenesis of head and neck squamous cell carcinoma. J Clin Investig. 2012; 122:1951–7. [PubMed: 22833868]

[4]. Marsh D, Suchak K, Moutasim KA, Vallath S, Hopper C, Jerjes W, et al. Stromal features are predictive of disease mortality in oral cancer patients. J Pathol. 2011; 223:470–81. [PubMed: 21294121]

[5]. Haddad RI, Shin DM. Recent advances in head and neck cancer. New Engl J Med. 2008; 359:1143–54. [PubMed: 18784104]

[6]. Opitz OG, Harada H, Suliman Y, Rhoades B, Sharpless NE, Kent R, et al. A mouse model of human oral-esophageal cancer. J Clin Investig. 2002; 110:761–9. [PubMed: 12235107]

[7]. Szaniszlo P, Fennewald SM, Qiu S, Kantara C, Shilagard T, Vargas G, et al. Temporal characterization of lymphatic metastasis in an orthotopic mouse model of oral cancer. Head Neck. 2013

[8]. Masood R, Hochstim C, Cervenka B, Zu S, Baniwal SK, Patel V, et al. A novel orthotopic mouse model of head and neck cancer and lymph node metastasis. Oncogenesis. 2013; 2:e68. [PubMed: 24018643]

[9]. Sano D, Myers JN. Xenograft models of head and neck cancers. Head Neck Oncol. 2009; 1:32. [PubMed: 19678942]

[10]. Killion JJ, Radinsky R, Fidler IJ. Orthotopic models are necessary to predict therapy of transplantable tumors in mice. Cancer Metast Rev. 1998; 17:279–84.

[11]. Sano D, Choi S, Milas ZL, Zhou G, Galer CE, Su YW, et al. The effect of combination anti-endothelial growth factor receptor and anti-vascular endothelial growth factor receptor 2 targeted therapy on lymph node metastasis: a study in an orthotopic nude mouse model of squamous cell carcinoma of the oral tongue. Archives Otolaryngol – Head Neck Surgery. 2009; 135:411–20.

[12]. Myers JN, Holsinger FC, Jasser SA, Bekele BN, Fidler IJ. An orthotopic nude mouse model of oral tongue squamous cell carcinoma. Clin Cancer Res: Off J Am Assoc Cancer Res. 2002; 8:293–8.

[13]. Kowalski LP, Carvalho AL, Martins Priante AV, Magrin J. Predictive factors for distant metastasis from oral and oropharyngeal squamous cell carcinoma. Oral Oncol. 2005; 41:534–41. [PubMed: 15878760]

[14]. Ferlito A, Shaha AR, Silver CE, Rinaldo A, Mondin V. Incidence and sites of distant metastases from head and neck cancer. ORL, J Oto-Rhino-Laryngol Relat Spec. 2001; 63:202–7.

[15]. Bhandari V, Jain RK. A retrospective study of incidence of bone metastasis in head and neck cancer. J Cancer Res Ther. 2013; 9:90–3. [PubMed: 23575081]

[16]. Smeets R, Grosjean MB, Heiland M, Riediger D, Maciejewski O. Distant metastases of a squamous cell carcinoma of the tongue in peripheral skeletal muscles and adjacent soft tissues. Head Face Med. 2008; 4:7. [PubMed: 18366774]

[17]. Dwivedi RC, Kazi R, Agrawal N, Chisholm E, Rose S St, Elmiyeh B, et al. Comprehensive review of small bowel metastasis from head and neck squamous cell carcinoma. Oral Oncol. 2010; 46:330–5. [PubMed: 20189444]

[18]. Bais MV, Ozdener GB, Sonenshein GE, Trackman PC. Effects of tumorsuppressor lysyl oxidase propeptide on prostate cancer xenograft growth and its direct interactions with DNA repair pathways. Oncogene. 2014 0.

[19]. Bais MV, Wigner N, Young M, Toholka R, Graves DT, Morgan EF, et al. BMP2 is essential for post natal osteogenesis but not for recruitment of osteogenic stem cells. Bone. 2009; 45:254–66. [PubMed: 19398045]

Author Manuscript Author Manuscript Author Manuscript Author Manuscript

[20]. Sengupta PK, Bouchie MP, Nita-Lazar M, Yang HY, Kukuruzinska MA. Coordinate regulation of N-glycosylation gene DPAGT1, canonical Wnt signaling and E-cadherin adhesion. J Cell Sci. 2013; 126:484–96. [PubMed: 23178939]

[21]. Wu Y, Wang Y, Yang XH, Kang T, Zhao Y, Wang C, et al. The deubiquitinase USP28 stabilizes LSD1 and confers stem-cell-like traits to breast cancer cells. Cell Reports. 2013; 5:224–36. [PubMed: 24075993]

[22]. Wang Y, Zhang H, Chen Y, Sun Y, Yang F, Yu W, et al. LSD1 is a subunit of the NuRD complex and targets the metastasis programs in breast cancer. Cell. 2009; 138:660–72. [PubMed: 19703393]

[23]. Lv T, Yuan D, Miao X, Lv Y, Zhan P, Shen X, et al. Over-expression of LSD1 promotes proliferation, migration and invasion in non-small cell lung cancer. PLoS ONE. 2012; 7:e35065. [PubMed: 22493729]

[24]. Ding J, Zhang ZM, Xia Y, Liao GQ, Pan Y, Liu S, et al. LSD1-mediated epigenetic modification contributes to proliferation and metastasis of colon cancer. Br J Cancer. 2013; 109:994–1003. [PubMed: 23900215]

[25]. Amente S, Lania L, Majello B. The histone LSD1 demethylase in stemness and cancer transcription programs. Biochim Biophys Acta. 2013; 1829:981–6. [PubMed: 23684752]

[26]. Varelas X, Bouchie MP, Kukuruzinska MA. Protein N-glycosylation in oral cancer: dysregulated cellular networks among DPAGT1, E-cadherin adhesion and canonical Wnt signaling. Glycobiology. 2014; 24:579–91. [PubMed: 24742667]

[27]. Nita-Lazar M, Noonan V, Rebustini I, Walker J, Menko AS, Kukuruzinska MA. Overexpression of DPAGT1 leads to aberrant N-glycosylation of E-cadherin and cellular discohesion in oral cancer. Cancer Res. 2009; 69:5673–80. [PubMed: 19549906]

[28]. Lin ZY, Chuang YH, Chuang WL. Cancer-associated fibroblasts up-regulate CCL2, CCL26, IL6 and LOXL2 genes related to promotion of cancer progression in hepatocellular carcinoma cells. Biomed Pharmaco = Biomed Pharmaco. 2012; 66:525–9.

[29]. Ahn SG, Dong SM, Oshima A, Kim WH, Lee HM, Lee SA, et al. LOXL2 expression is associated with invasiveness and negatively influences survival in breast cancer patients. Breast Cancer Res Treat. 2013; 141:89–99. [PubMed: 23933800]

[30]. Peng L, Ran YL, Hu H, Yu L, Liu Q, Zhou Z, et al. Secreted LOXL2 is a novel therapeutic target that promotes gastric cancer metastasis via the Src/FAK pathway. Carcinogenesis. 2009; 30:1660–9. [PubMed: 19625348]

[31]. Lu H, Hu L, Yu L, Wang X, Urvalek AM, Li T, et al. KLF8 and FAK cooperatively enrich the active MMP14 on the cell surface required for the metastatic progression of breast cancer. Oncogene. 2014; 33:2909–17. [PubMed: 23812425]

[32]. Akanuma N, Hoshino I, Akutsu Y, Murakami K, Isozaki Y, Maruyama T, et al. MicroRNA-133a regulates the mRNAs of two invadopodia-related proteins, FSCN1 and MMP14, in esophageal cancer. Br J Cancer. 2014; 110:189–98. [PubMed: 24196787]

[33]. Xu M, Wang YZ. MiR133a suppresses cell proliferation, migration and invasion in human lung cancer by targeting MMP14. Oncol Rep. 2013; 30:1398–404. [PubMed: 23783274]

[34]. Bibby MC. Orthotopic models of cancer for preclinical drug evaluation: advantages and disadvantages. Eur J Cancer. 2004; 40:852–7. [PubMed: 15120041]

[35]. Hawkins BL, Heniford BW, Ackermann DM, Leonberger M, Martinez SA, Hendler FJ. 4NQO carcinogenesis: a mouse model of oral cavity squamous cell carcinoma. Head Neck. 1994; 16:424–32. [PubMed: 7960739]

[36]. Schoop RA, Noteborn MH, Baatenburg de Jong RJ. A mouse model for oral squamous cell carcinoma. J Mol Histol. 2009; 40:177–81. [PubMed: 19685146]

[37]. Kim S. Animal models of cancer in the head and neck region. Clin Exp Otorhinolaryngol. 2009; 2:55–60. [PubMed: 19565028]

[38]. Konstantinopoulos PA, Matulonis UA. Current status and evolution of preclinical drug development models of epithelial ovarian cancer. Frontiers Oncol. 2013; 3:296.

Author Manuscript Author Manuscript Author Manuscript Author Manuscript

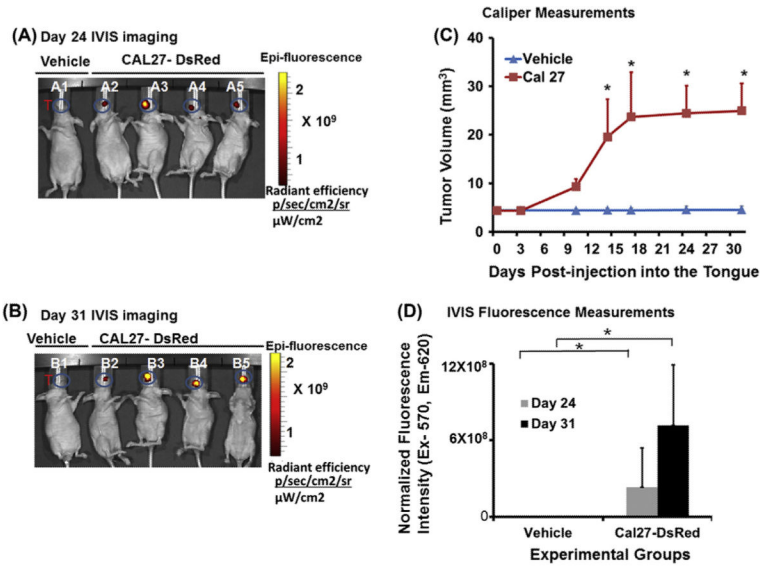

Fig. 1.

Orthotopic injection of CAL27 cell induces tongue tumor in nude mice. Orthotopic tongue tumors were generated by injecting CAL27 cells expressing DsRed into the tongue of nude mice ($n = 5$), and imaged by an *in vivo* Live imaging system (IVIS 200) at regular intervals starting at day 7 to day 31. Control mice ($n = 5$) were injected with vehicle. (A) *In vivo* imaging of CAL27-DsRed injected mice shows primary tongue tumor growth 24 days post injection; lane A1 represents nude mice injected with vehicle whereas lanes A2–A5 show mice injected with CAL27-DsRed cells (T represents region of interest of tongue for quantification of fluorescence intensity); (B) *in vivo* imaging of CAL27-DsRed cells injected into the tongue shows tumor growth 31 days post injection; lane B1 represents nude mice injected with vehicle only whereas lane B2–B5 shows mice injected with CAL27-DsRed cells (T represents region of interest of tongue for quantification of fluorescence intensity); (C) caliper measurements at different internals show growth of tongue tumors, but not in vehicle-injected mice ($n = 5$; $^{*}P < 0.05$, $^{*}P < 0.01$; 2-way ANOVA) and (D) quantification and normalization of fluorescence intensity data for IVIS imaging at day 24 and day 31 ($n = 5$; $*P < 0.01$; 2-way ANOVA).

Author Manuscript Author Manuscript Author Manuscript Author Manuscript

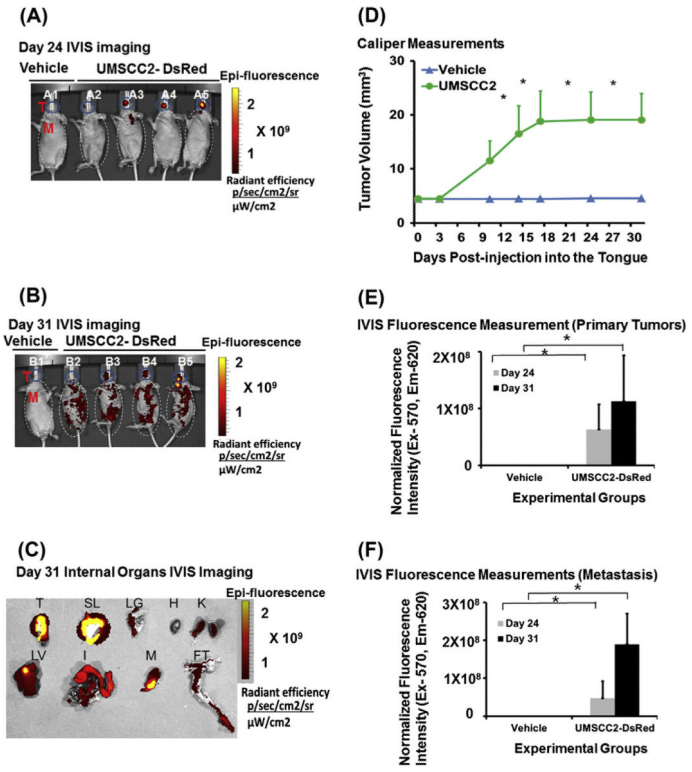

Fig. 2.

Orthotopic injection of UMSCC2 cells induces primary tumor and spontaneous metastasis in nude mice. Orthotopic tongue tumors were generated by injecting UMSCC2 cells expressing DsRed into the tongues of nude mice ($n = 5$) and imaged with an *in vivo* Live Imaging System (IVIS 200) at regular interval starting at day 7 to day 31. Control mice ($n = 5$) were injected with vehicle. (A) *In vivo* imaging of UMSCC2-DsRed cells injected tongues shows primary tumor growth 24 days post injection; the lane B1 represents nude mice injected with vehicle only and lanes B2–B5 show mice injected with CAL27-DsRed cells (T and M represents region of interest of tongue and metastasis of other organs for quantification of fluorescence intensity, respectively); (B) *in vivo* imaging of UMSCC2-DsRed cells injected shows primary tongue tumor growth 31 days post injection; lane C1 represents nude mice injected with vehicle only whereas lanes C2–C5 show mice injected with UMSCC2-DsRed cells (T and M represents region of interest of tongue and metastasis of other organs for quantification of fluorescence intensity, respectively); (C) fluorescence imaging of internal organs after necropsy shows the presence of UMSCC2 cells (T = tongue; SL = sublingual tissue including salivary gland; LG = lung; H = heart; K = kidneys; LV = Liver; I = Intestine; M = Mandible and FT = femur and tibia); (D) caliper measurements at different internals shows growth of tongue tumors, but not in vehicle-injected mice ($n = 5$; $^{*}P < 0.01$; 2-way ANOVA); (E) quantification and normalization of fluorescence intensity data for IVIS imaging at day 24 and day 31 ($n = 5$; $^{*}P < 0.01$; 2-way ANOVA) and (F) quantification of metastasis by fluorescence intensity data for IVIS imaging at day 24 and day 31 ($n = 5$; $^{*}P < 0.01$; 2-way ANOVA).

Author Manuscript Author Manuscript Author Manuscript Author Manuscript

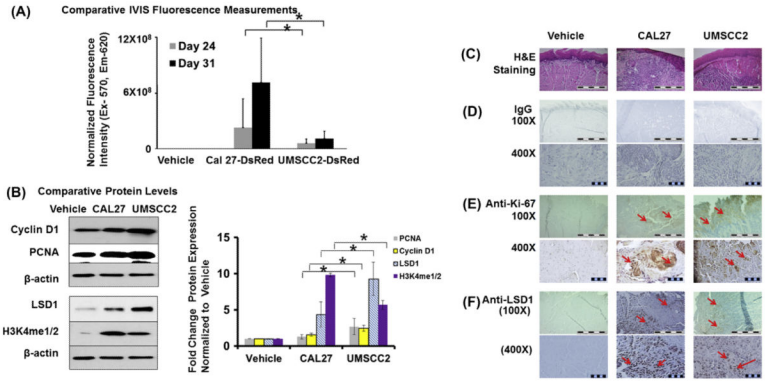

Fig. 3.

Comparison of CAL27 and UMSCC2 induced primary tumors. (A) Quantification of fluorescence imaging shows differences in intensity of Cal 27 and UMSCC2 induced tumors ($n = 5$; $^{*}P < 0.05$, $^{*}P < 0.01$; 2-way ANOVA) and (B) western blot analysis and quantification of, Cyclin D1, PCNA, LSD1 and H3K4Me1/2 compared to respective β-actin from tissue extracts ($n = 3$; $^{*}P < 0.05$, $^{*}P < 0.01$; 2-way ANOVA) and (C) H & E staining (100X) from tissue sections injected with UMSCC2 and CAL27 compared to vehicle are shown. immunostaining with (D) non-immune IgG control (100X and 400X), (E) anti-Ki-67 antibody (100X and 400X) and (F) anti-LSD1 antibody (100X and 400X) of tongue tumors sections in vehicle, CAL27 and UMSCC2 injection groups; scale bar = 1 mm for 100X and 0.1 mm for 400X.

Author Manuscript Author Manuscript Author Manuscript Author Manuscript

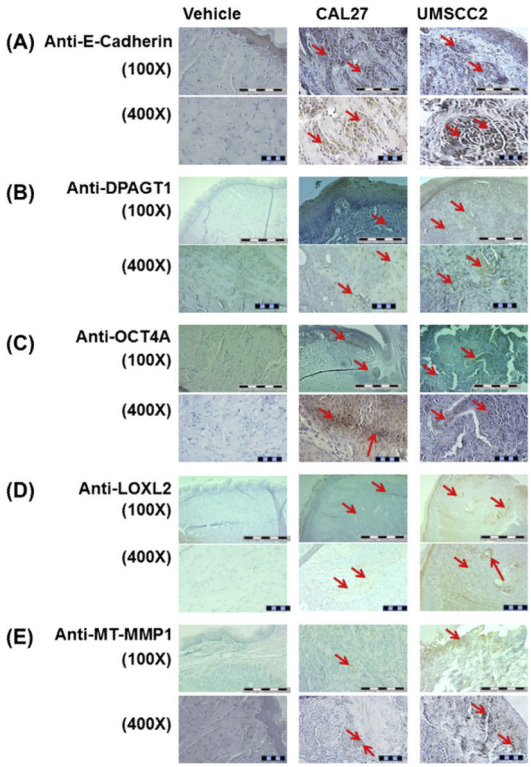

Fig. 4.

Characterization of CAL27 and UMSCC2 induced primary tumors by immunostaining with OSCC related protein expression. Immunostaining with (A) E-cadherin antibody (100X and 400X), (B) DPAGT1 antibody (100X and 400X), (C) anti-OCT4A antibody (100X and 400X), (D) anti-LOXL2 antibody (100X and 400X) and (E) MT-MMP1 antibody (100X and 400X) of tongue tumors sections in vehicle, CAL27 and UMSCC2 injection groups; scale bar = 1 mm for 100X and 0.1 mm for 400X.